JOURNAL of
MATERIALS and MECHATRONICS:A

e-ISSN 2717-8811
JournalMM, 2025, 6(1), 83-102
https://doi.org/10.55546/jmm.1610751

Araştırma Makalesi / Research Article

Thermomechanical Buckling Behavior of FGM Sandwich Nanoplate with Honeycomb Core Based on NSGT

Adem Fatih OZALP*

* Karabuk University, Faculty of Engineering, Department of Mechanical Engineering, Karabuk, Türkiye,
ORCID ID: https://orcid.org/0000-0001-8873-4663, ademfatihozalp@kbu.edu.tr

Geliş/ Received: 31.12.2024**;** **Revize/Revised:** 16.02.2025 **Kabul / Accepted:** 27.02.2025

ABSTRACT: This study investigates the nondimensional buckling behavior of a functionally graded material (FGM) sandwich nanoplate. The analysis consider variations in material gradation parameter, length ratio, thickness ratio, incline angle, nonlocal parameter and size parameter. Higher-order shear deformation theory (HSDT), Nonlocal strain gradient theory (NSGT), Hamilton's principle, and the Navier solution with simply supported boundary conditions are employed to derive and solve the governing equations of motion. The effects of nonlocal elasticity, strain gradient elasticity, dimension change of the core layer on the thermomechanical buckling behavior of the sandwich nanoplate have been examined in a broad framework. It is observed that the thickness ratio and incline angle in the core layer are effective on the thermomechanical buckling behavior of the sandwich nanoplate whereas length ratio change has a neglectable results. Material gradation parameter changes buckling behavior significantly. The research provides critical conclusions for the design of FG nanoplates in advanced thermal and mechanical applications, emphasizing the adjustability of buckling behavior via material and structural modifications.

Keywords: Sandwich nanoplate, Honeycomb, Ti-6Al-4V, Al_2O_3, Thermomechanical buckling

*Sorumlu yazar / Corresponding author: ademfatihozalp@kbu.edu.tr
Bu makaleye atıf yapmak için /To cite this article

Ozalp, A. F. (2025). Thermomechanical Buckling Behavior of FGM Sandwich Nanoplate with Honeycomb Core Based on NSGT. Journal of Materials and Mechatronics: A (JournalMM), 6(1), 83-102.

1. INTRODUCTION

FGMs are abundantly studied by researchers for their significant and unique resistance to environmental conditions. FGMs are researched in many different structure types such as plate, beam, hollow pipe, sphere or as shell to these specific structure types (Abuteir and Boutagouga, 2022; Akgöz and Civalek, 2014; Chen et al., 2022; Ozalp and Esen, 2025). These models are used as helpful for the production of dental applications, space technology, smart nanoelectromechanical systems, nanosensors, and invisibility technology.

FGMs are not just produced as one material as they are produced of generally metal and ceramic materials in terms of different volumes along the thickness. This characteristic of FGMs features a distinct and specific response to environmental conditions compared to composites. Also FGMs can be used with different structure types such as a plate with pure metal foam core between two FGM surface layers (Al-Waily et al., 2022). Additionally, honeycomb can be used instead of foam core and supply different results for different conditions.

Because of its cellular design, honeycomb structures have special mechanical qualities that enable effective distribution of load and energy absorption. Geometric setup, material anisotropy, and temperature fluctuations all affect these structures' thermal buckling response. For instance, the angle parameter of honeycomb cell will have the largest load capacity. This can be seen in the nanobeam's lowest level of displacement and its highest level of critical buckling stress. Different results are obtained with auxetic honeycomb structures compared to materials with positive Poisson's ratios. These structures have variable stiffness and negative Poisson's ratios, which are affected by their geometric features (Van Lieu et al., 2024).

FGMs are made with different properties that can be changed to lower stress levels and make them more resistant to heat. A lot of research has been conducted on the thermal buckling of cylindrical shells with FGM coatings. This studies show how defective cylinder shells react to thermal stress (Dang et al., 2024; Wang et al., 2016). The results show that the difference in the material's properties has a big effect on the critical buckling temperature. This shows that FGMs can make honeycomb structures more resistant to heat. The addition of auxetic materials to honeycomb constructions is very helpful in situations where high energy absorption and structural resilience are needed.

One important feature of honeycomb structures is how they change when they are hit. Experiments are conducted to assess the damage patterns that happen when high-speed impact hit honeycomb sandwich structures with FGM face plates (Arslan and Gunes, 2018). The test results showed that changing the FGM face plates' material makeup changed the types of damage they could take, how much energy they could absorb, and how well they could withstand impacts. There was also energy absorption from the honeycomb core through plastic buckling of the cell walls and lateral crushing deformations.

Spaceship bus designs should make designs more flexible and lighter without sacrificing functionality. To keep the needed rigidity while minimizing mass, a spacecraft structure needs to be very efficient. Because they are light, stiff, and strong in bending, honeycomb sandwich shapes are being used more and more in industry (Boudjemai et al., 2013).

Modern computing methods, like finite element analysis (FEA), have led to more about how honeycomb FGM plates react to temperature changes. The study of how new re-entrant circular auxetic honeycombs react to dynamic crushing shows how accurate numerical models can be at predicting what complex structures will behave under different loading conditions. Results show that

design factors might make honeycomb-FGM structures work better in terms of heat and force (Qi et al., 2022).

Biological tissues, including bone, wood, and sponge, demonstrate hierarchical cellular structures that are lightweight and exhibit enhanced energy absorption properties. A study on bio-inspired hierarchical honeycombs demonstrates the ability of these materials to exhibit improved reliability and energy absorption characteristics (Yin et al., 2018). Plates also can be utilized in many areas at nanoscale such as nanocardboard could be used as a structural element for scanning probe cantilevers, microflyer or interstellar lightsail wings, and other microscopic and macroscopic systems (Lin et al., 2018)

Mentioned literature reveals that the examination of FG surface plates with honeycomb core sandwich structures affected by temperature forms a relatively unexplored research area. Recent studies have concentrated on these structures because of the remarkable mechanical and thermal properties associated with honeycomb configurations. Honeycomb structures, due to their metamaterial characteristics, have the potential for novel applications in various fields. This study examines the thermomechanical buckling properties of composite nanoplates, consisting of a honeycomb core layer and FG metal/ceramic surface layers. This research provides a comprehensive analysis of the thermomechanical buckling response of sandwich nanoplates, with findings presented in detail. The investigation's results demonstrated that the buckling response of the sandwich nanoplate can be substantially altered to meet defined conditions and requirements. The findings of this study will contribute to important application areas, such as aerospace and submarine vehicles, which need protection against ultrasonic and mechanical waves in both standard and high temperature conditions. The results obtained are expected to be relevant for radar stealth applications and for the protection of nanoelectromechanical systems operating in high noise and vibration environments.

2. FG NANOPLATE SANDWICH STRUCTURE

Figure 1 presents a schematic representation of the sandwich nanoplate under investigation, while Figure 2 depicts core layer structure comprised of honeycomb. The sandwich structure consists of a honeycomb core layer (Ti-6Al-4V) between top and bottom FGM layers (Ti-6Al-4V; Al_2O_3).

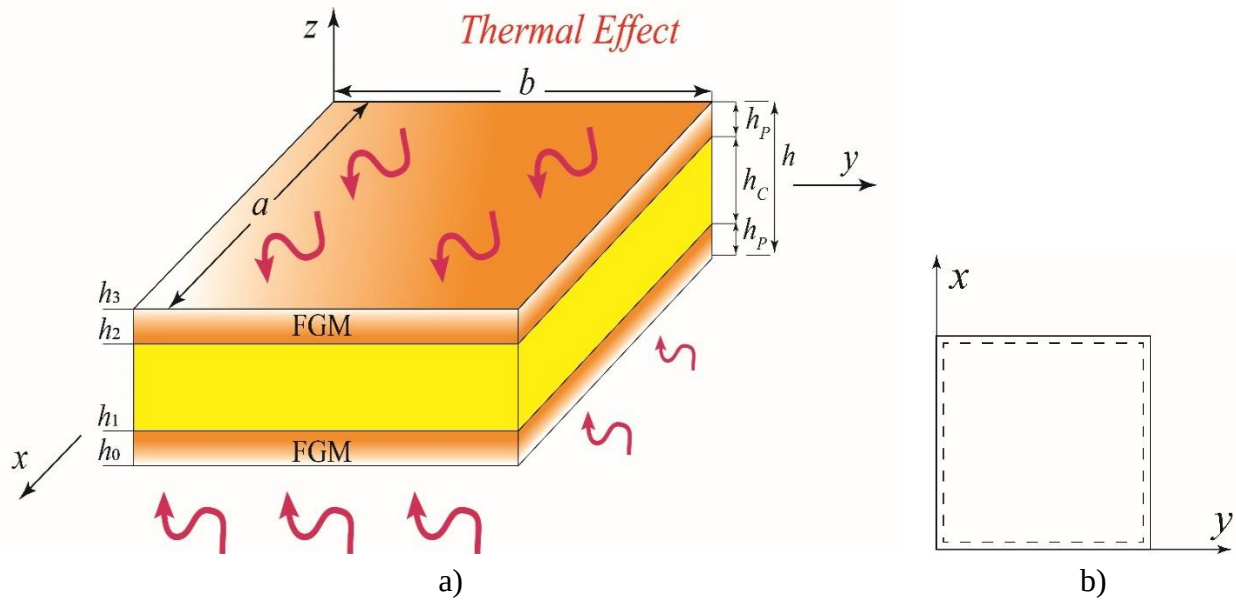

Figure 1. (a) Top and bottom FGM plates with honeycomb core (b) SSSS plate boundary conditions

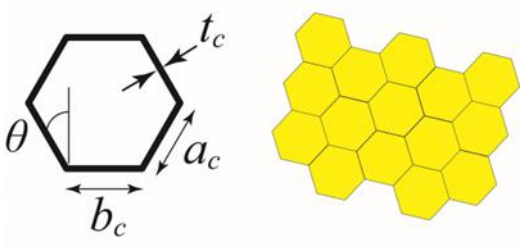

Figure 2. Honeycomb core layer and dimension symbols

2.1 Core Layer

Gibson formula (Gibson, 2003) is used to find the properties of honeycomb layer changing with structural dimensions as follows:

$$E_{11} = \frac{E_c {\zeta_3}^3 \cos\theta}{(\zeta_1 + \sin\theta)\sin^2\theta}\left[1 - {\zeta_3}^2 \cot^2\theta\right] \tag{1}$$

$$E_{22} = \frac{E_c {\zeta_3}^3 (\zeta_1 + \sin\theta)}{\cos^3\theta}\left[1 - {\zeta_3}^2 (\zeta_1 \sec^2\theta + \tan^2\theta)\right] \tag{2}$$

$$E_{33} = \frac{E_c \zeta_3 (2 + \zeta_1)}{2(\zeta_1 + \sin\theta)\cos\theta} \tag{3}$$

$$v_{12} = \frac{\cos^2\theta}{(\zeta_1 + \sin\theta)\sin\theta}\left[1 - {\zeta_3}^2 \csc^2\theta\right] \tag{4}$$

$$G_{12} = \frac{E_c {\zeta_3}^3 (\zeta_1 + \sin\theta)}{{\zeta_1}^2 (1 + 2\zeta_1)\cos\theta} \tag{5}$$

$$G_{13} = \frac{G_c \zeta_3 \cos\theta}{\zeta_1 + \sin\theta} \tag{6}$$

$$G_{23} = \frac{G_c \zeta_3}{2\cos\theta}\left[\frac{\zeta_1 + \sin\theta}{(1 + 2\zeta_1)\cos\theta} + \frac{\zeta_1 + 2\sin^2\theta}{2(\zeta_1 + \sin\theta)}\right] \tag{7}$$

$$\rho^c = \frac{\rho_{TiAlV} \zeta_3 (\zeta_1 + 2)}{2\cos\theta(\zeta_1 + \sin\theta)} \tag{8}$$

$$\alpha^c = \frac{\alpha_{TiAlV} \zeta_3 (\zeta_1 + 2)}{2\cos\theta(\zeta_1 + \sin\theta)} \tag{9}$$

$$\psi^c = \frac{\psi_{TiAlV} \zeta_3 (\zeta_1 + 2)}{2\cos\theta(\zeta_1 + \sin\theta)} \tag{10}$$

$$\zeta_1 = \frac{b_c}{a_c} \tag{11}$$

$$\zeta_3 = \frac{t_c}{a_c} \tag{12}$$

$G_{ij,ik,jk}$, v_{ij}, $E_{ii,jj}$ and ρ denote Shear moduli, Poisson's ratio, Elastic modulus, and density, respectively, for the hexagonal core. ψ denotes the thermal conductivity coefficient while α is thermal expansion coefficient. Coefficient subscript c stands for the honeycomb material (eg., E_c as Elastic moduli). For other honeycomb coefficients, a_c, b_c, and t_c denote inclined lengths, vertical length and thickness of the cell rib respectively, while θ represents the inclination degree. ζ_1 denotes length ratio and ζ_3 represents thickness ratio (Figure 1, 2).

2.2 FGM Face Layers

Numerous distribution functions have been proposed in the literature for the simulation of FGM structures (Touloukian, 1967). This research examines the applied Voigt model (Markworth et al., 1995).

Top layer:

$$P(z) = [P_m - P_c]V_c + P_m, \qquad V_c = \left(\frac{z}{h} + \frac{1}{2}\right)^p, \qquad V_c + V_m = 1, \qquad h_2 < z < h_3 \tag{13a}$$

Bottom layer:

$$P(z) = [P_c - P_m]V_m + P_c, \qquad V_m = \left(\frac{z}{h} + \frac{1}{2}\right)^p, \qquad V_c + V_m = 1, \qquad h_0 < z < h_1 \tag{13b}$$

Each layer can have a different P(z) which symbolizes effective material parameter and it changes along the z-direction. P_c stands for the properties of ceramic constituent and P_m denotes metal property characteristics. The volume fraction of the ceramic material is represented by V_c and V_m correspond to ceramic and metal material, also the power distribution, denoted as p, ranges from zero to infinity. In the condition of p=∞, the layer completely contains metal, but at p=0, it purely contains ceramic (Equation 13a, 13b). From h_0 to h_1 are the boundaries of bottom plate thickness and from h_2 to h_3 is defined as top plate thickness boundaries. For the core plate thickness boundaries range from h_1 to h_2.

The calculation of temperature dependent material coefficients can be conducted using a nonlinear temperature function (Table 1), as accounting for the temperature effect is crucial for precise predictions of the structure's behavior (Markworth et al., 1995).

$$P_i = P_0\,(P_{-1}T^{-1} + 1 + P_1T + P_2T^2 + P_3T^3) \tag{14}$$

The characteristics of each material are determined by its P_i (i=0,1,2,3) values, corresponding to various temperature (T) values.

2.3 The Temperature Effect

To find uniform, linear and nonlinear temperature rise in the equation, FG nanoplate temperature is raised to its final temperature in the condition of initial temperature is T_0=300K and plate is stress-free.

$$\Delta T = T - T_0 \tag{15}$$

Based on the assumption that the temperature increases linearly (LTR) from T_t to T_b across the thicknesses, the temperature of a horizontal surface that extends in the z-axis with the temperatures of its bottom and upper surfaces, T_b and T_t, respectively, can be computed as follows (Kiani and Eslami, 2013):

$$T(z) = T_b + (T_t - T_b)\left(\frac{h + 2z}{2h}\right) \tag{16}$$

Table 1. Temperature dependent coefficients of the FG sandwich plate (Reddy and Chin, 1998)

Material	Property	P_{-1}	P_0	P_1	P_2	P_3
Ti-6Al-4V	E(Pa)	0	122.56x10^{9}	-4.586x10^{-4}	0	0
	v	0	0.2884	1.121x10^{-4}	0	0
	$\alpha(\mathrm{K}^{-1})$	0	7.5788x10^{-6}	6.638x10^{-4}	-3.147x10^{-6}	0
	ψ(W/mK)	0	1.000	1.704x10^{-2}	0	0
	$\rho(\mathrm{kg/m^3})$	0	4420	0	0	0
Al_2O_3	E(Pa)	0	349.55 x10^{9}	-3.853 x10^{-4}	4.027 x10^{-7}	-1.673 x10^{-10}
	v	0	0.26	0	0	0
	$\alpha(\mathrm{K}^{-1})$	0	6.8269 x10^{-6}	1.838 x10^{-4}	0	0
	ψ(W/mK)	-1123.6	-14.087	-6.227 x10^{-3}	0	0
	$\rho(\mathrm{kg/m^3})$	0	3750	0	0	0

The one-dimensional heat transfer problem can be analyzed under conditions of a nonlinear temperature increase (NLTR) across the thickness of the nanoplates, utilizing defined temperature boundary limits to determine the upper and lower surface temperatures (T_b and T_t) of the plate (Ozalp and Esen, 2024).

$$-\frac{d}{dz}\left(\psi(z)\frac{dT}{dz}\right) = 0, \qquad T\left(\frac{h}{2}\right) = T_t, \quad T\left(-\frac{h}{2}\right) = T_b \tag{17}$$

ψ represents the thermal conductivity coefficient. The temperature at any position along the thickness of the *z*-axis, given a specific boundary condition, can be determined as follows:

$$T(z) = T_b + (T_t - T_b)\frac{\int_{-\frac{h}{2}}^{z}\frac{1}{\psi(z,T)}dz}{\int_{-\frac{h}{2}}^{\frac{h}{2}}\frac{1}{\psi(z,T)}d(z)} \tag{18}$$

2.4 Application of Nonlocal Strain Gradient Elasticity

The calculations for shear and normal stresses at any particular position can be performed using σ_{xx}^{t} and σ_{xz}^{t} the total stress in the *xz* and *xy* directions as follows (Arani, 2017):

$$\begin{aligned}\sigma_{xx}^{t} &= \sigma_{xx}^{c} - \nabla^2\sigma_{xx}^{h}\\ \sigma_{xz}^{t} &= \sigma_{xz}^{c} - \nabla^2\sigma_{xz}^{h}\end{aligned} \tag{19}$$

Where:

$$\sigma_{xx}^{c} = \int_{V} E(z)\alpha_0(\boldsymbol{x}', \boldsymbol{x}, e_0 a)\varepsilon'_{xx}(\boldsymbol{x}')dV' \tag{20a}$$

$$\sigma_{xx}^{h} = l_m^2 \int_{V} E(z)\alpha_1(\boldsymbol{x}', \boldsymbol{x}, e_1 a)\nabla\varepsilon'_{xx}(\boldsymbol{x}')dV' \tag{20b}$$

$$\sigma_{xz}^{c} = \int_{V} G(z)\alpha_0(\boldsymbol{x}', \boldsymbol{x}, e_0 a)\varepsilon'_{xz}(\boldsymbol{x}')dV' \tag{20c}$$

$$\sigma_{xz}^{h} = l_m^2 \int_{V} G(z)\alpha_1(\boldsymbol{x}', \boldsymbol{x}, e_1 a)\nabla\varepsilon'_{xz}(\boldsymbol{x}')dV' \tag{20d}$$

Here, σ^c and σ^h represent the normal and shear stresses of higher-order and classical types, with ∇ utilized as the Laplacian operator. Additionally, the size parameter l_m quantifies the impact of size at the nanoscale. The functions $\alpha_0\ (\boldsymbol{x}', \boldsymbol{x}, e_0 a)$ and $\alpha_1\ (\boldsymbol{x}', \boldsymbol{x}, e_1 a)$ denote the nonlocal weakening functions associated with the strains ε'_{xx} and ε'_{xz}. Additionally, V signifies volume. The nonlocality coefficients are represented as e_0 and e_1 (Arani and Jalaei, 2017). Assuming $e_0 = e_1$, and utilizing a linear differential operator, we can derive the next equation pertaining to the Nonlocal Strain Gradient Theory (NSGT) (Lim et al., 2015):

$$\left[1 - (e_0 a)^2 \nabla^2\right]\sigma_{xx}^{t} = [1 - l_m^2\nabla^2]E(z)\varepsilon_{xx} \tag{21a}$$

$$\left[1 - (e_0 a)^2 \nabla^2\right]\sigma_{xz}^{t} = [1 - l_m^2\nabla^2]G(z)\varepsilon_{xz} \tag{21b}$$

where ε_{xx} denotes normal strain, γ_{xz} signifies the shear strain, and σ^t represents the total stress:

$$\sigma_{xx}^{t} - (e_0 a)^2 \frac{\partial^2 \sigma_{xx}^{t}}{\partial x^2} = \left[\varepsilon_{xx} - l_m^2 \frac{\partial^2 \varepsilon_{xx}}{\partial x^2}\right] E(z) \tag{22a}$$

$$\sigma_{xz}^{t} - (e_0 a)^2 \frac{\partial^2 \sigma_{xz}^{t}}{\partial x^2} = \left[\gamma_{xz} - l_m^2 \frac{\partial^2 \gamma_{xz}}{\partial x^2}\right] G(z) \tag{22b}$$

2.5 Displacement Fields and Strains

The HSDT (Shimpi, 2002) is developed based on the subsequent assumptions:

$$u_1(x, y, z, t) = u(x, y, t) - z\frac{\partial w_b}{\partial x} - f(z)\frac{\partial w_s}{\partial x} \tag{23a}$$

$$u_2(x, y, z, t) = v(x, y, t) - z\frac{\partial w_b}{\partial y} - f(z)\frac{\partial w_s}{\partial y} \tag{23b}$$

$$u_3(x, y, z, t) = w_b(x, y, t) + w_s(x, y, t) \tag{23c}$$

Here, $f(z) = -z/4 + 5z^3/3h^2$. The displacements along the coordinate directions (x, y, z) are represented by u_1, u_2, u_3. The variables u and v indicate the displacements of a point on the midplane along the x and y directions. For the transverse displacement, w_s is shear component and w_b is bending component. The variable h signifies the thickness length. The HSDT, as stated earlier, neglects the effect of the thickness stretching considering a uniform transverse displacement throughout the thickness. The displacement field in equation (23c) is altered by integrating

supplementary variables addressing the thickness stretching that signifies the transverse displacement.

$$u_3(x,y,z,t) = w_b(x,y,t) + w_s(x,y,t) + g(z)w_z(x,y,t) \tag{24}$$

The displacement function w_z denotes an unspecified function that accounts for the influence of thickness stretching. The shape function $g(z)$ is established in accordance with the stress-free boundary conditions at the upper and lower surfaces of the nanoplate. Utilizing the same methods described by Reddy, the form function $g(z)$ is derived as (Reddy, 1984):

$$g(z) = 1 - f'(z) = \frac{5}{4}\left(1 - \frac{4z^2}{h^2}\right) \tag{25}$$

The linear strains associated with the newly established displacement field in equations (23, 24) are as follows:

$$\varepsilon_{xx} = \frac{\partial u}{\partial x} - z\frac{\partial^2 w_b}{\partial x^2} - f(z)\frac{\partial^2 w_s}{\partial x^2} \tag{26a}$$

$$\varepsilon_{yy} = \frac{\partial v}{\partial y} - z\frac{\partial^2 w_b}{\partial y^2} - f(z)\frac{\partial^2 w_s}{\partial y^2} \tag{26b}$$

$$\varepsilon_z = g'(z)w_z \tag{26c}$$

$$\gamma_{xy} = \frac{\partial u}{\partial y} + \frac{\partial v}{\partial x} - 2z\frac{\partial^2 w_b}{\partial x\,\partial y} - 2f(z)\frac{\partial^2 w_s}{\partial x\,\partial y} \tag{26d}$$

$$\gamma_{xz} = g(z)\left(\frac{\partial w_s}{\partial x} + \frac{\partial w_z}{\partial x}\right) \tag{26e}$$

$$\gamma_{yz} = g(z)\left(\frac{\partial w_s}{\partial y} + \frac{\partial w_z}{\partial y}\right) \tag{26f}$$

The tensions develop due to constitutive interactions.

$$\begin{bmatrix}\sigma_x\\ \sigma_y\\ \sigma_z\\ \sigma_{xy}\\ \sigma_{xz}\\ \sigma_{yz}\end{bmatrix} = \frac{1}{E(z)}\begin{bmatrix}1 & -v & -v & 0 & 0 & 0\\ -v & 1 & -v & 0 & 0 & 0\\ -v & -v & 1 & 0 & 0 & 0\\ 0 & 0 & 0 & 2(1+v) & 0 & 0\\ 0 & 0 & 0 & 0 & 2(1+v) & 0\\ 0 & 0 & 0 & 0 & 0 & 2(1+v)\end{bmatrix}\begin{bmatrix}\varepsilon_{xx}\\ \varepsilon_{yy}\\ \varepsilon_{zz}\\ \gamma_{xy}\\ \gamma_{xz}\\ \gamma_{yz}\end{bmatrix} + \alpha\Delta T\begin{bmatrix}1\\1\\1\\0\\0\\0\end{bmatrix} \tag{27}$$

C_{ijkl} represents the three-dimensional elastic constants.

$$\varepsilon_{ij} = \frac{(1+v)}{E(z)}\sigma_{ij} - \frac{v}{E(z)}\sigma_{kk}\gamma_{ij} + \alpha\Delta T\gamma_{ij} \tag{28a}$$

$$\sigma_{ij} = \frac{E(z)}{1+v}\left\{\varepsilon_{ij} + \frac{v}{(1-2v)}\right\} - \frac{E\alpha\Delta T}{1-2v}\gamma_{ij} \tag{28b}$$

$$\sigma_{ij} = C_{ijkl}(\varepsilon_{kl} - \alpha\Delta T\delta_{kl}) \text{ and } \varepsilon_{ij} = S_{ijkl}\sigma_{kl} - \alpha\Delta T\gamma_{ij} \tag{28c}$$

$$C_{ijkl} = \frac{E(z)}{2(1+v)}(\gamma_{il}\gamma_{jk} + \gamma_{ik}\gamma_{jl}) + \frac{vE(z)}{(1-2v)(1+v)}\gamma_{ij}\gamma_{kl} \tag{28d}$$

$$S_{ijkl} = \frac{(1+v)}{2E(z)}(\gamma_{il}\gamma_{jk} + \gamma_{ik}\gamma_{jl}) - \frac{v}{E(z)}\gamma_{ij}\gamma_{kl} \tag{28e}$$

In the absence of the thickness stretching effect (i.e., ε_z=0), Equation (27) is modified for constitutive relations as follows:

$$\begin{bmatrix}\sigma_x\\ \sigma_y\\ \sigma_{xy}\\ \sigma_{yz}\\ \sigma_{xz}\end{bmatrix} = \frac{E}{1-v^2}\begin{bmatrix}1 & v & 0 & 0 & 0\\ v & 1 & 0 & 0 & 0\\ 0 & 0 & \frac{(1-v)}{2} & 0 & 0\\ 0 & 0 & 0 & \frac{(1-v)}{2} & 0\\ 0 & 0 & 0 & 0 & \frac{(1-v)}{2}\end{bmatrix}\begin{bmatrix}\varepsilon_x\\ \varepsilon_y\\ \gamma_{xy}\\ \gamma_{yz}\\ \gamma_{xz}\end{bmatrix} + \frac{E\alpha\Delta T}{1-2v}\begin{bmatrix}1\\1\\1\\0\\0\\0\end{bmatrix} \tag{29}$$

Given the negligible influence of Poisson's ratio on the response of FG plates (Kitipornchai et al., 2006; Yang et al., 2005), it is assumed to be constant for simplicity. This study suggests that elastic moduli exhibits variation throughout the nanoplate thickness, following a power-law distribution based on the volume fraction of the constituents.

The mathematical expression for the strain energy of the nanoplate is as follows:

$$U = \frac{1}{2}\int_A \left(\sum_{n=1}^{3}\int_{h_{n-1}}^{h_n}\left(\sigma_x\varepsilon_x + \sigma_y\varepsilon_y + \sigma_z\varepsilon_z + \sigma_{xy}\gamma_{xy} + \sigma_{xz}\gamma_{xz} + \sigma_{yz}\gamma_{yz}\right)dz\right)dA \tag{30}$$

The area is denoted by A. By replacing equation (26) into equation (27) and subsequently applying the results in equation (30) allows for the reformulation of the strain energy expression as:

$$U = \frac{1}{2}\int_A \begin{pmatrix} N_x\frac{\partial u}{\partial x} - M_x^b\frac{\partial^2 w_b}{\partial x^2} - M_x^s\frac{\partial^2 w_s}{\partial x^2} + N_y\frac{\partial v}{\partial y} - M_y^b\frac{\partial^2 w_b}{\partial y^2} - M_y^s\frac{\partial^2 w_s}{\partial y^2} + R_z w_z \\ +N_{xy}\left(\frac{\partial u}{\partial y} + \frac{\partial v}{\partial x}\right) - 2M_{xy}^b\frac{\partial^2 w_b}{\partial x\,\partial y} - 2M_{xy}^s\frac{\partial^2 w_s}{\partial x\,\partial y} + Q_x\left(\frac{\partial w_b}{\partial x} + \frac{\partial w_z}{\partial x}\right) + Q_y\left(\frac{\partial w_s}{\partial y} + \frac{\partial w_z}{\partial y}\right) \end{pmatrix} dA \tag{31}$$

Here *N*, *M*, *Q*, and *R* represent the specified stress resultants.

$$\left(N_x, N_y, N_{xy}\right) = \sum_{n=1}^{3}\int_{h_{n-1}}^{h_n}\left(\sigma_x, \sigma_y, \sigma_{xy}\right)dz \tag{32a}$$

$$\left(M_x^b, M_y^b, M_{xy}^b\right) = \sum_{n=1}^{3}\int_{h_{n-1}}^{h_n}\left(\sigma_x, \sigma_y, \sigma_{xy}\right)dz \tag{32b}$$

$$\left(M_x^s, M_y^s, M_{xy}^s\right) = \sum_{n=1}^{3}\int_{h_{n-1}}^{h_n}\left(\sigma_x, \sigma_y, \sigma_{xy}\right)f(z)dz \tag{32c}$$

$$\left(Q_x, Q_y\right) = \sum_{n=1}^{3} \int_{h_{n-1}}^{h_n} \left(\sigma_{xz}, \sigma_{yz}\right) g(z) dz \tag{32d}$$

$$R_z = \sum_{n=1}^{3} \int_{h_{n-1}}^{h_n} \sigma_z g'(z) dz \tag{32e}$$

Replacing equation (25) into equation (26) and subsequently incorporating the resulting values into equation (32) allows for the representation of stress resultants in the form of displacement components (u, v, w_b, w_s, w_z).

$$N_x = A_{11}\frac{\partial u}{\partial x} + A_{12}\frac{\partial v}{\partial y} - B_{11}\frac{\partial^2 w_b}{\partial x^2} - B_{12}\frac{\partial^2 w_b}{\partial y^2} - B_{11}^s\frac{\partial^2 w_s}{\partial x^2} - B_{12}^s\frac{\partial^2 w_s}{\partial y^2} + X_{13}w_z \tag{33a}$$

$$N_y = A_{12}\frac{\partial u}{\partial x} + A_{22}\frac{\partial v}{\partial y} - B_{12}\frac{\partial^2 w_b}{\partial x^2} - B_{22}\frac{\partial^2 w_b}{\partial y^2} - B_{12}^s\frac{\partial^2 w_s}{\partial x^2} - B_{22}^s\frac{\partial^2 w_s}{\partial y^2} + X_{23}w_z \tag{33b}$$

$$N_{xy} = A_{66}\left(\frac{\partial u}{\partial y} + \frac{\partial v}{\partial x}\right) - 2B_{66}\frac{\partial^2 w_b}{\partial x\,\partial y} - 2B_{66}^s\frac{\partial^2 w_s}{\partial x\,\partial y} \tag{33c}$$

$$M_x^b = B_{11}\frac{\partial u}{\partial x} + B_{12}\frac{\partial v}{\partial y} - D_{11}\frac{\partial^2 w_b}{\partial x^2} - D_{12}\frac{\partial^2 w_b}{\partial y^2} - D_{11}^s\frac{\partial^2 w_s}{\partial x^2} \tag{33d}$$

$$M_y^b = B_{12}\frac{\partial u}{\partial x} + B_{22}\frac{\partial v}{\partial y} - D_{12}\frac{\partial^2 w_b}{\partial x^2} - D_{22}\frac{\partial^2 w_b}{\partial y^2} - D_{12}^s\frac{\partial^2 w_s}{\partial x^2} - D_{22}^s\frac{\partial^2 w_s}{\partial y^2} + Y_{23}w_z \tag{33e}$$

$$R_z = \sum_{n=1}^{3} \int_{h_{n-1}}^{h_n} \sigma_z g'(z) dz \tag{33f}$$

$$M_x^s = B_{11}^s\frac{\partial u}{\partial x} + B_{12}^s\frac{\partial v}{\partial y} - D_{11}^s\frac{\partial^2 w_b}{\partial x^2} - D_{12}^s\frac{\partial^2 w_b}{\partial y^2} - H_{11}^s\frac{\partial^2 w_s}{\partial x^2} - H_{12}^s\frac{\partial^2 w_s}{\partial y^2} + Y_{13}^s w_z \tag{33g}$$

$$M_y^s = B_{12}^s\frac{\partial u}{\partial x} + B_{22}^s\frac{\partial v}{\partial y} - D_{12}^s\frac{\partial^2 w_b}{\partial x^2} - D_{22}^s\frac{\partial^2 w_b}{\partial y^2} - H_{12}^s\frac{\partial^2 w_s}{\partial x^2} - H_{22}^s\frac{\partial^2 w_s}{\partial y^2} + Y_{23}^s w_z \tag{33h}$$

$$M_{xy}^s = B_{66}^s\left(\frac{\partial u}{\partial y} + \frac{\partial v}{\partial x}\right) - 2D_{66}^s\frac{\partial^2 w_b}{\partial x\,\partial y} - 2H_{66}^s\frac{\partial^2 w_s}{\partial x\,\partial y} \tag{33i}$$

$$R_z = X_{13}\frac{\partial u}{\partial x} + X_{23}\frac{\partial v}{\partial y} - Y_{13}\frac{\partial^2 w_b}{\partial x^2} - Y_{23}\frac{\partial^2 w_b}{\partial y^2} - Y_{13}^s\frac{\partial^2 w_s}{\partial x^2} - Y_{23}^s\frac{\partial^2 w_s}{\partial y^2} + Z_{33}w_z \tag{33j}$$

$$Q_x = A_{55}^s\left(\frac{\partial w_s}{\partial x} + \frac{\partial w_z}{\partial x}\right), \quad Q_y = A_{44}^s\left(\frac{\partial w_s}{\partial y} + \frac{\partial w_z}{\partial y}\right) \tag{33k}$$

Where

$$\left(A_{ij}, A_{ij}^s, B_{ij}, B_{ij}^s, D_{ij}, D_{ij}^s, H_{ij}^s\right) = \sum_{n=1}^{3} \int_{h_{n-1}}^{h_n} (1, g^2, z, f, z^2, fz, f^2) C_{ij} dz \tag{34}$$

$$\left(X_{ij}, Y_{ij}, Y_{ij}^s, Z_{ij}\right) = \sum_{n=1}^{3} \int_{h_{n-1}}^{h_n} (g', g'z, g'f, g'^2) C_{ij} dz \tag{35}$$

The effects of transverse loads q which are externally applied can be expressed as follows:

$$V = -\int_A q(w_b + w_s + gw_z)\, dA \tag{36}$$

The expression for kinetic energy is:

$$K = \frac{1}{2}\int_A \left(\sum_{n=1}^{3}\int_{h_{n-1}}^{h_n} \rho(\dot{u}_1^2 + \dot{u}_2^2 + \dot{u}_3^2)dz\right) dA \tag{37}$$

The axial force due to temperature variation is specified for both directions.

$$N_{xx}^T = \mathrm{b}\sum_{n=1}^{3}\int_{h_{n-1}}^{h_n} (Q_{11})\, \alpha^{(n)}(z)T(z)dz \tag{38a}$$

$$N_{yy}^T = \mathrm{a}\sum_{n=1}^{3}\int_{h_{n-1}}^{h_n} (Q_{11})\, \alpha^{(n)}(z)T(z)dz \tag{38b}$$

From the mid-plane distance (*z*) at a particular layer (*n*); the variable $\alpha^{(n)}$ denotes coefficient of thermal expansion of the FG sandwich plate. Q_{11} represents the honeycomb core elastic moduli. The external potential energy of thermal loads and in-plane mechanical loads are N_{ox} and N_{oy}:

$$V = \int_\Omega \left[(-N_{ox} - N_{xx}^T)\left(w_{b,xx} + w_{s,xx}\right) + \left(-N_{oy} - N_{yy}^T\right)\left(w_{b,yy} + w_{s,yy}\right)\right] d\Omega \tag{39}$$

Where $w_{b,xx} = \frac{\partial^2 w_b}{\partial x^2}$, $w_{b,yy} = \frac{\partial^2 w_b}{\partial y^2}$, $w_{s,xx} = \frac{\partial^2 w_s}{\partial x^2}$, $w_{s,yy} = \frac{\partial^2 w_s}{\partial y^2}$

Here, Hamilton's principle is applied to determine the equations of motion. The following is an analytical expression for the principle:

$$\int_0^T \delta(U + V - K)\, dt = 0 \tag{40}$$

The variational operator is δ. Replacing the formulas for *U*, *V*, and *K* from equations (23, 24, 37, 39) into equation (40), integrating, and collecting the coefficients of (δu, δv, δw_b, δw_s, δw_z) yields the subsequent motion equations as:

$$\delta u: \frac{\partial N_x}{\partial x} + \frac{\partial N_{xy}}{\partial y} = I_0\ddot{u} - I_1\frac{\partial \ddot{w}_b}{\partial x} - J_1\frac{\partial \ddot{w}_s}{\partial x} \tag{41a}$$

$$\delta v: \frac{\partial N_{xy}}{\partial x} + \frac{\partial N_y}{\partial y} = I_0\ddot{v} - I_1\frac{\partial \ddot{w}_b}{\partial y} - J_1\frac{\partial \ddot{w}_s}{\partial y} \tag{41b}$$

$$\begin{aligned}\delta w_b: \frac{\partial^2 M_x^b}{\partial x^2} + 2\frac{\partial^2 M_{xy}^b}{\partial x\,\partial y} + \frac{\partial^2 M_y^b}{\partial y^2} - q + (N_{xx}^T + N_{ox})\left(w_{b,xx} + w_{s,xx}\right) \\ + \left(N_{yy}^T + N_{oy}\right)\left(w_{b,yy} + w_{s,yy}\right) \\ = I_0(\ddot{w}_b + \ddot{w}_s) + J_0\ddot{w}_z + I_1\left(\frac{\partial \ddot{u}}{\partial x} + \frac{\partial \ddot{v}}{\partial y}\right) - I_2\nabla^2\ddot{w}_b - J_2\nabla^2\ddot{w}_s\end{aligned} \tag{41c}$$

$$\begin{aligned}\delta w_s: \frac{\partial^2 M_x^s}{\partial x^2} + 2\frac{\partial^2 M_{xy}^s}{\partial x\,\partial y} + \frac{\partial^2 M_y^s}{\partial y^2} + \frac{\partial Q_{xz}}{\partial x} + \frac{\partial Q_{yz}}{\partial y} - q + (N_{xx}^T + N_{ox})w_{0,xx} \\ + \left(N_{yy}^T + N_{oy}\right)\left(w_{b,yy} + w_{s,yy}\right)\end{aligned} \tag{41d}$$

$$\begin{aligned}\delta w_z: \frac{\partial Q_{xz}}{\partial x} + \frac{\partial Q_{yz}}{\partial y} - R_z - gq + (N_{xx}^T + N_{ox})\left(w_{b,xx} + w_{s,xx}\right) + \left(N_{yy}^T + N_{oy}\right)\left(w_{b,yy} + w_{s,yy}\right) \\ = J_0(\ddot{w}_b + \ddot{w}_s) + K_0\ddot{w}_z\end{aligned} \tag{41e}$$

The following is the definition of the mass moments of inertia, which are denoted by I_i, J_i, K_i.

$$(I_0, I_1, I_2) = \sum_{n=1}^{3}\int_{h_{n-1}}^{h_n}(1, z, z^2)\rho dz \tag{42a}$$

$$(J_0, J_1, J_2) = \sum_{n=1}^{3}\int_{h_{n-1}}^{h_n}(g, f, fz)\rho dz \tag{42b}$$

$$(K_0, K_1, K_2) = \sum_{n=1}^{3}\int_{h_{n-1}}^{h_n}(g, f, fz)\rho dz \tag{42c}$$

Using HSDT, the motion equations are generated by equation (41) if the influence of thickness stretching effect is ignored (w_z=0) (Thai and Choi, 2011; Thai; Thai and Choi, 2012; Thai, et al., 2012).

Replacing equation (27) into equation (32) allows for the expression of the motion equations in forms of displacements (u, v, w_b, w_s, w_z).

$$\mathfrak{B} = \left(1 - (l_m)^2\nabla^2\right) \tag{43a}$$

$$\mathfrak{D} = \left(1 - (e_0 a)^2\nabla^2\right) \tag{43b}$$

$$\begin{aligned}\mathfrak{B}\Bigg(A_{11}\frac{\partial^2 u}{\partial x^2} + A_{66}\frac{\partial^2 u}{\partial y^2} + (A_{12} + A_{66})\frac{\partial^2 v}{\partial x\,\partial y} - B_{11}\frac{\partial^3 w_b}{\partial x^3} - (B_{12} + 2B_{66})\frac{\partial^3 w_b}{\partial x\,\partial y^2} \\ -B_{11}^s\frac{\partial^3 w_s}{\partial x^3} - (B_{12}^s + 2B_{66}^s)\frac{\partial^3 w_s}{\partial x\,\partial y^2} + X_{13}\frac{\partial w_z}{\partial x}\Bigg) \\ = \mathfrak{D}\left(I_0\ddot{u} - I_1\frac{\partial \ddot{w}_b}{\partial x} - J_1\frac{\partial \ddot{w}_s}{\partial x}\right)\end{aligned} \tag{43c}$$

$$\mathfrak{B}\begin{pmatrix} A_{22}\dfrac{\partial^2 v}{\partial y^2} + A_{66}\dfrac{\partial^2 v}{\partial x^2} + (A_{12} + A_{66})\dfrac{\partial^2 u}{\partial x\,\partial y} - B_{22}\dfrac{\partial^3 w_b}{\partial y^3} \\ -(B_{12} + 2B_{66})\dfrac{\partial^3 w_b}{\partial x^2\,\partial y} + B_{22}\dfrac{\partial^3 v_s}{\partial y^3} - (B_{12}^s + 2B_{66}^s)\dfrac{\partial^3 w_b}{\partial x^2\,\partial y} + X_{13}\dfrac{\partial w_z}{\partial y}\end{pmatrix} \tag{43d}$$

$$= \mathfrak{D}\left(I_0\ddot{v} - I_1\frac{\partial\ddot{w}_b}{\partial y} - J_1\frac{\partial\ddot{w}_s}{\partial y}\right)$$

$$\mathfrak{B}\begin{pmatrix} B_{11}\frac{\partial^3 u}{\partial x^3} + (B_{12}+2B_{66})\left(\frac{\partial^3 u}{\partial x\,\partial y^2} + \frac{\partial^3 v}{\partial x^2\,\partial y}\right) + B_{22}\frac{\partial^3 v}{\partial y^3} - D_{11}\frac{\partial^4 w_b}{\partial x^4} \\ -D_{22}\frac{\partial^4 w_b}{\partial y^4} - 2(D_{12}+2D_{66})\frac{\partial^4 w_b}{\partial x^2\,\partial y^2} - D_{11}^s\frac{\partial^4 w_s}{\partial x^4} - D_{22}^s\frac{\partial^4 w_s}{\partial y^4} \\ -2(D_{12}^s+2D_{66}^s)\frac{\partial^4 w_s}{\partial x^2\,\partial y^2} + Y_{13}\frac{\partial^2 w_z}{\partial x^2} + Y_{23}\frac{\partial^2 w_z}{\partial y^2} + q \end{pmatrix} \tag{43e}$$
$$= \mathfrak{D}\begin{pmatrix} -I_2\nabla^2\ddot{w}_b - J_2\nabla^2\ddot{w}_s + I_0(\ddot{w}_b+\ddot{w}_s) + J_0\ddot{w}_z - I_1\left(\frac{\partial\ddot{w}}{\partial x} + \frac{\partial\ddot{v}}{\partial y}\right) \\ -q + (N_{xx}^T + N_{ox})\left(w_{b,xx}+w_{s,xx}\right) + \left(N_{yy}^T + N_{oy}\right)\left(w_{b,yy}+w_{s,yy}\right) \end{pmatrix}$$

$$\mathfrak{B}\begin{pmatrix} B_{11}^s\frac{\partial^3 u}{\partial x^3} + (B_{12}^s+2B_{66}^s)\left(\frac{\partial^3 u}{\partial x\,\partial y^2} + \frac{\partial^3 v}{\partial x^2\,\partial y}\right) + B_{22}^s\frac{\partial^3 v}{\partial y^3} - D_{11}^s\frac{\partial^4 w_b}{\partial x^4} \\ -D_{22}^s\frac{\partial^4 w_b}{\partial y^4} - 2(D_{12}^s+2D_{66}^s)\frac{\partial^4 w_b}{\partial x^2\,\partial y^2} - H_{11}^s\frac{\partial^4 w_s}{\partial x^4} \\ -H_{22}^s\frac{\partial^4 w_s}{\partial y^4} - 2(H_{12}^s+2H_{66}^s)\frac{\partial^4 w_s}{\partial x^2\,\partial y^2} + A_{55}^s\frac{\partial^2 w_s}{\partial x^2} + A_{44}^s\frac{\partial^2 w_s}{\partial y^2} \\ +(Y_{13}^s+A_{55}^s)\frac{\partial^2 w_z}{\partial x^2} + (Y_{23}^s+A_{44}^s)\frac{\partial^2 w_z}{\partial y^2} + q \end{pmatrix} \tag{43f}$$
$$= \mathfrak{D}\begin{pmatrix} I_0(\ddot{w}_b+\ddot{w}_s) - J_0\ddot{w}_z + J_1\left(\frac{\partial\ddot{w}_s}{\partial x} + \frac{\partial\ddot{v}_s}{\partial y}\right) - J_2\ddot{w}_b\nabla^2 - K_2\ddot{w}_s\nabla^2 - q \\ +(N_{xx}^T + N_{ox})\left(w_{b,xx}+w_{s,xx}\right) + \left(N_{yy}^T + N_{oy}\right)\left(w_{b,yy}+w_{s,yy}\right) \end{pmatrix}$$

$$\mathfrak{B}\begin{pmatrix} -X_{13}\frac{\partial u}{\partial x} - X_{23}\frac{\partial v}{\partial y} + Y_{13}\frac{\partial^2 w_b}{\partial x^2} + Y_{23}\frac{\partial^2 w_b}{\partial y^2} + (Y_{13}^s+A_{55}^s)\frac{\partial^2 w_s}{\partial x^2} \\ +(Y_{23}^s+A_{44}^s)\frac{\partial^2 w_s}{\partial y^2} + A_{55}^s\frac{\partial^2 w_z}{\partial x^2} + A_{44}^s\frac{\partial^2 w_z}{\partial y^2} - Z_{33}w_z \end{pmatrix} \tag{43g}$$
$$= \mathfrak{D}\begin{pmatrix} J_0(\ddot{w}_b+\ddot{w}_s) + (N_{xx}^T + N_{ox})\left(w_{b,xx}+w_{s,xx}\right) \\ +K_0\ddot{w}_z + \left(N_{yy}^T + N_{oy}\right)\left(w_{b,yy}+w_{s,yy}\right) \end{pmatrix}$$

2.6 Closed-Form Solutions

The Navier method is used to get the analytical solutions to equation (43) for simply supported plates. The Navier approach states as follows:

$$u(x,y,t) = \sum_{m=1}^{\infty}\sum_{n=1}^{\infty} U_{mn}e^{i\omega t}\cos\alpha x\sin\beta y \tag{44a}$$

$$v(x,y,t) = \sum_{m=1}^{\infty}\sum_{n=1}^{\infty} V_{mn}e^{i\omega t}\sin\alpha x\cos\beta y \tag{44b}$$

$$w_b(x,y,t) = \sum_{m=1}^{\infty}\sum_{n=1}^{\infty} W_{bmn} e^{i\omega t} \sin\alpha x \sin\beta y \tag{44c}$$

$$w_s(x,y,t) = \sum_{m=1}^{\infty}\sum_{n=1}^{\infty} W_{smn} e^{i\omega t} \sin\alpha x \sin\beta y \tag{44d}$$

$$w_z(x,y,t) = \sum_{m=1}^{\infty}\sum_{n=1}^{\infty} W_{zmn} e^{i\omega t} \sin\alpha x \sin\beta y \tag{44e}$$

Here, $i = \sqrt{-1},\ \alpha = m\pi/a,\ \beta = n\pi/b.$ The coefficients are denoted as $(U_{mn}, V_{mn}, W_{bmn}, W_{smn}, W_{zmn})$. In this context, ω denotes the angular frequency. A modification in the double-Fourier sine series is used to represent the transverse load q.

$$q(x,y) = \sum_{m=1}^{\infty}\sum_{n=1}^{\infty} Q_{mn} \sin\alpha x \sin\beta y \tag{45}$$

The following lists the coefficients Q_{mn} for a number of sample loads:

$$\begin{aligned} Q_{mn} &= \frac{4}{ab}\int_0^a \int_0^b q(x,y)\sin\alpha x \sin\beta y \, dxdy \\ &= \begin{cases} q_0 & \text{for sinusoidally distributed load} \\ \dfrac{16q_0}{mn\pi^2} & \text{for uniformly distributed load} \end{cases} \end{aligned} \tag{46}$$

The uniform distributed load is denoted as q_0. The closed-form solutions can be obtained by replacing equation (43), with equations (44, 45).

When the thickness stretching effect is eliminated (i.e., ε_z =0), the precise HSDT solutions are given as (Thai and Choi, 2011; Thai; Thai and Choi, 2012; Thai, et al., 2012).:

$$\left(\begin{bmatrix} k_{11} & k_{12} & k_{13} & k_{14} & k_{15} \\ k_{12} & k_{22} & k_{23} & k_{24} & k_{25} \\ k_{13} & k_{23} & k_{33} & k_{34} & k_{35} \\ k_{14} & k_{24} & k_{34} & k_{44} & k_{45} \\ k_{15} & k_{25} & k_{35} & k_{45} & k_{55} \end{bmatrix} - \omega^2 \begin{bmatrix} m_{11} & 0 & m_{13} & m_{14} & 0 \\ 0 & m_{22} & m_{23} & m_{24} & 0 \\ m_{13} & m_{23} & m_{33} & m_{34} & m_{35} \\ m_{14} & m_{24} & m_{34} & m_{44} & m_{45} \\ 0 & 0 & m_{35} & m_{45} & m_{55} \end{bmatrix}\right) \begin{bmatrix} U_{mn} \\ V_{mn} \\ W_{bmn} \\ W_{smn} \\ W_{zmn} \end{bmatrix} = \begin{bmatrix} 0 \\ 0 \\ Q_{mn} \\ Q_{mn} \\ 0 \end{bmatrix} \tag{47}$$

Where

$$k_{11} = A\left(\alpha^2 + \frac{1-v}{2}\beta^2\right)c_2, \qquad k_{12} = \frac{1+v}{2}A\alpha\beta c_2 \tag{48a}$$

$$k_{22} = A\left(\frac{1-v}{2}\alpha^2 + \beta^2\right)c_2, \quad k_{13} = -B\alpha(\alpha^2+\beta^2)c_2 \tag{48b}$$

$$k_{13} = -B\alpha(\alpha^2+\beta^2)c_2, \qquad k_{14} = -B^s\alpha(\alpha^2+\beta^2)c_2 \tag{48c}$$

$$k_{14} = -B^s\alpha(\alpha^2+\beta^2)c_2, \qquad k_{23} = -B\beta(\alpha^2+\beta^2)c_2 \tag{48d}$$

$$k_{24} = -B^s\beta(\alpha^2+\beta^2)c_2, \qquad k_{33} = D(\alpha^2+\beta^2)^2c_2 + \epsilon \tag{48e}$$

$$k_{34} = D^s(\alpha^2+\beta^2)^2c_2 + \epsilon, \qquad k_{44} = \left(H(\alpha^2+\beta^2)^2 + A^s(\alpha^2+\beta^2)\right)c_2 + \epsilon \tag{48f}$$

$$m_{11} = m_{22} = I_0 c_1, \qquad m_{13} = m_{14} = -\alpha I_1 c_1 \tag{48g}$$

$$m_{23} = m_{24} = -\beta I_1 c_1, m_{33} = I_0 + I_2(\alpha^2 + \beta^2)c_1 \tag{48h}$$

$$m_{34} = I_0 + J_2(\alpha^2 + \beta^2)c_1, \qquad m_{44} = I_0 + K_2(\alpha^2 + \beta^2)c_1 \tag{48i}$$

$$\epsilon = \left(-q + (N_{xx}^T + N_{ox})\alpha^2 + \left(N_{yy}^T + N_{oy}\right)\beta^2\right)c_1 \tag{48j}$$

$$c_1 = \left(1 + (e_0 a)^2\right)(\alpha^2 + \beta^2), c_2 = \left(1 + (l_m)^2\right)(\alpha^2 + \beta^2) \tag{48k}$$

$$(A, B, B^s, D, D^s, H) = \sum_{n=1}^{3} \int_{h_{n-1}}^{h_n} (1, z, f, z^2, zf, f^2) \frac{E(z)}{1 - v^2} dz \tag{48l}$$

$$A^s = \sum_{n=1}^{3} \int_{h_{n-1}}^{h_n} \frac{g^2 E(z)}{2(1 + v)} dz \tag{48m}$$

The following is a condensed version of equation (49) for the buckling solution:

$$\begin{bmatrix} k_{11} & k_{12} & k_{13} & k_{14} & k_{15} \\ k_{12} & k_{22} & k_{23} & k_{24} & k_{25} \\ k_{13} & k_{23} & k_{33} & k_{34} & k_{35} \\ k_{14} & k_{24} & k_{34} & k_{44} & k_{45} \\ k_{15} & k_{25} & k_{35} & k_{45} & k_{55} \end{bmatrix} \begin{bmatrix} U_{mn} \\ V_{mn} \\ W_{bmn} \\ W_{smn} \\ W_{zmn} \end{bmatrix} = \begin{bmatrix} 0 \\ 0 \\ 0 \\ 0 \\ 0 \end{bmatrix} \tag{49a}$$

$$(\mathbf{K})\mathbf{d} = 0$$

With

$$\mathbf{d} = \begin{bmatrix} U_{mn} \\ V_{mn} \\ W_{bmn} \\ W_{smn} \\ W_{zmn} \end{bmatrix} \tag{49b}$$

The stiffness matrix **K** incorporates all thermal and external loads as specified in equation (48). By setting the determinant of **K** to zero, one can derive the critical buckling loads. When the **K** matrix equals zero, the thermal force terms are moved to the right, and the terms on the left are divided by the coefficients of the force terms to determine the critical buckling load $N_{cr}^T(m, n)$ as presented in equation (52).

$$(\mathbf{K})\mathbf{d} = 0 \tag{50}$$

$$N_{cr}^T(m, n) = \frac{\det(\mathbf{K}) - \Psi N^T}{\Psi} \tag{51}$$

Under the assumption that the determinant of the **K**=0, the entire set of coefficients for the thermal force of magnitude N^T in the equation is represented by the symbol Ψ.

The dimensionless buckling load of the modes (*m*, *n*) is represented by the following equation:

$$\lambda_{cr}(m,n) = \frac{12(1-v_c^2)N_{cr}a^2}{E_c h^3} \tag{52}$$

The critical buckling load is denoted by λ_{cr} and E_c is the ceramic material's elasticity moduli.

3. NUMERICAL RESULTS

A sandwich plate with the dimensions of a=b=L=500 nm, FG face-layers comprised of Ti-6Al-4V and Al_2O_3 with Ti-6Al-4V honeycomb is studied for the present study. The nondimensional buckling response λ_1 is observed according to applied thermal environment with the change of p, ζ_1, ζ_3, θ, $e_0 a$, l_m parameters.

It is observed that p rise in FG face plates drops down the buckling load λ_1 in Figure 3a. At p=0, 1, 2, 10, buckling temperatures are 2161 K, 2131 K, 2106 K, 2006 K respectively. Furthermore, at fixed temperature analysis with respect to p raise, p=0 shows higher buckling load results. p rise slopes down the dimensionless buckling load as it is seen in Figure 3b. Thermal expansion ratio directly affects the result as it is fully ceramic at p=0.

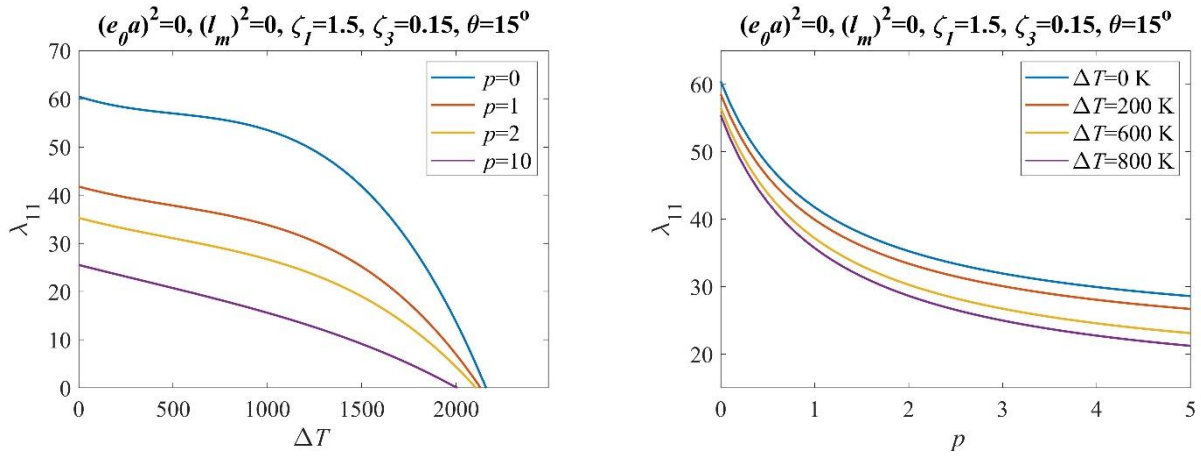

a) b)

Figure 3. Relationship between the dimensionless buckling load and (a) temperature rise for different values of p (0, 1, 2, 10), (b) material grading index p of face-plates (0-5) for different values of temperature rise (ΔT=0, 50, 100, 125 K); h_c=0.2h, h_p=0.4h, h=L/10

Increase in length ratio (ζ_1) doesn't affect the response of buckling load very much (Figure 4a), however thickness ratio rise (ζ_3) and especially incline angle (θ) rise directly change the λ_1 response (Figure 4b and 4c). After an intersection point, buckling load curve starts sloping down with increase of ζ_3. Before intersection point larger ζ_3 values cause higher buckling load. Unlike ζ_3, θ rise drops down the λ_1 response and after intersection point, λ_1 response rises together with θ rise.

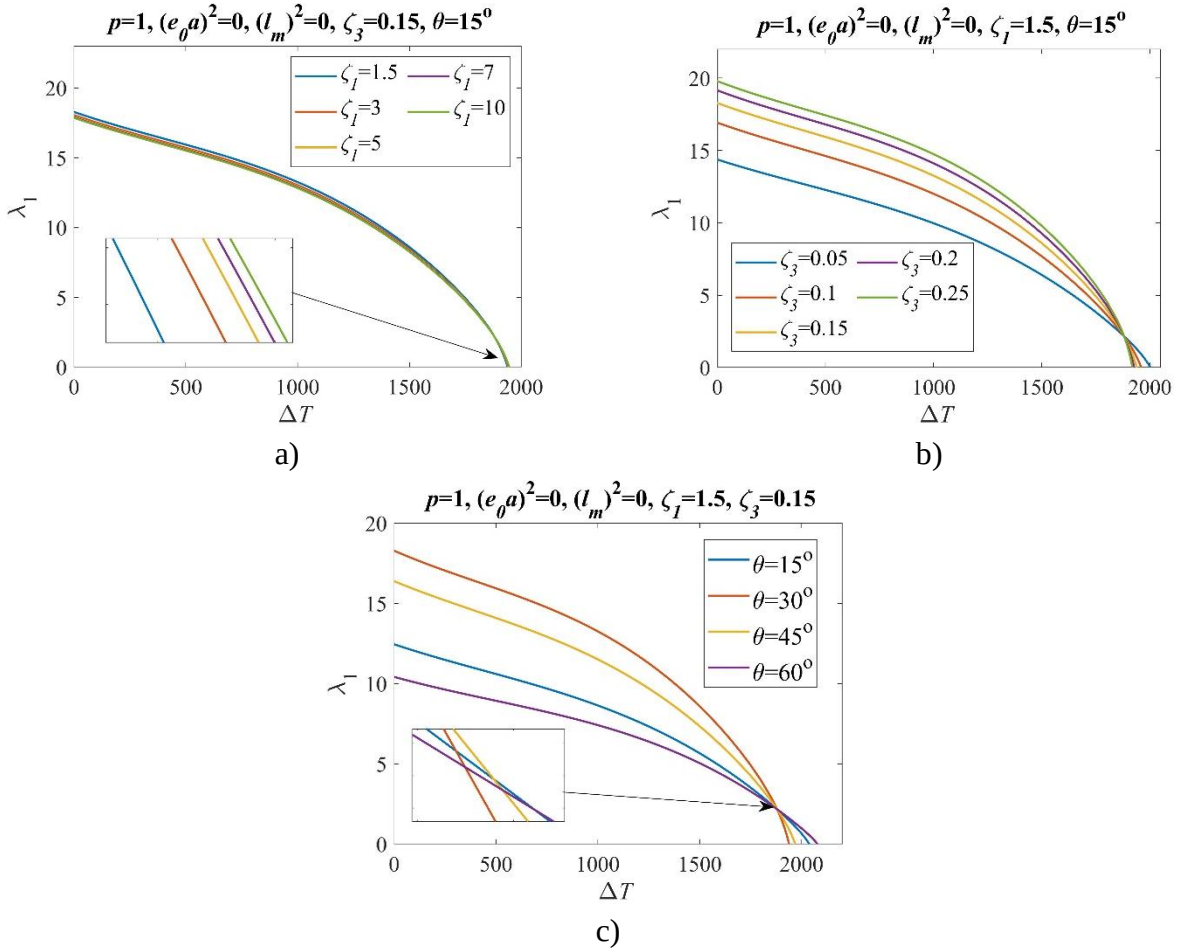

Figure 3. Relationship between the dimensionless buckling load and temperature rise for different values of (a) ζ_1=(1.5, 3, 5, 7, 10), (b) ζ_3=(0.05, 0.1, 0.15, 0.2, 0.25) (c) θ=(15°, 30°, 45°, 60°) ; h_c=0.8h, h_p=0.1h, h=L/10

At p=1 which is %50 Ti-6Al-4V and %50 Al_2O_3 constituent FG face layers, sandwich plate buckling load decreases with nonlocal parameter (e_0a) rise due to softening effect (Figure 5a). Unlike e_0a, size parameter (l_m) shows opposite results and l_m increases the λ_1 due to hardening effect. For $(e_0a)^2$=0, 1, 2, 4 nm^2 nondimensional buckling loads are 23.93, 19.98, 17.18, 13.37 at 1500 K, respectively. Additionally, for $(l_m)^2$=0, 1, 2, 4 nm^2 nondimensional buckling loads are 23.93, 28.65, 33.31, 42.81 at 1500 K respectively

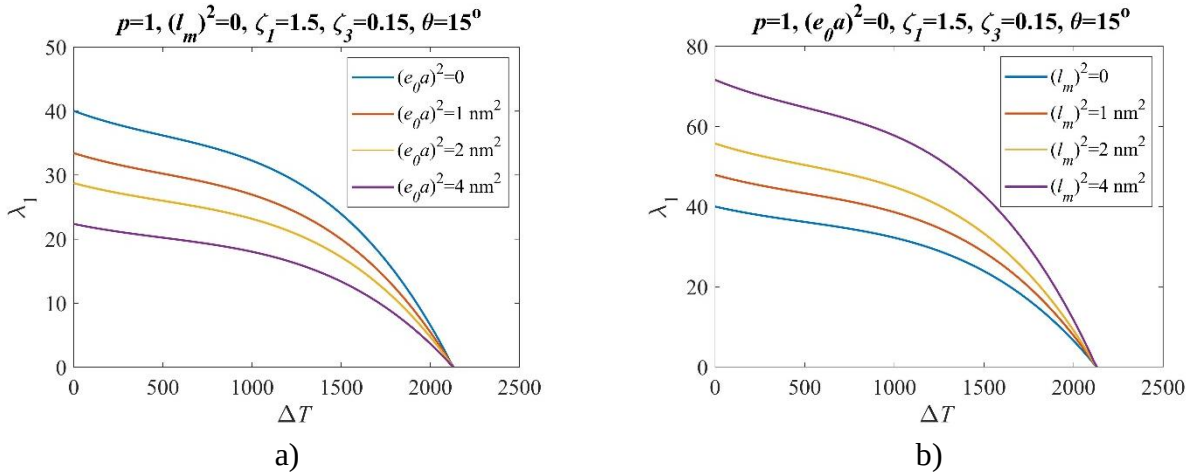

Figure 4. Relationship between the dimensionless buckling load and temperature rise for different values of (a) $(e_0a)^2$= (0, 1, 2, 4 nm^2), (b) $(l_m)^2$= (0, 1, 2, 4 nm^2); h_c=0.3h, h_p=0.35h, h=L/10.

4. CONCLUSIONS

A FGM sandwich nanoplate with honeycomb core layer and FG surface plates is analyzed in thermal environment to observe dimensionless buckling load according to changing parameters as p, ζ_1, ζ_3, θ, e_0a, l_m. For the solution higher-order shear deformation theory is considered. Using the Hamilton principle, the equations of motion of the plate are derived and written in terms of the displacement components. Assuming simply supported boundary conditions, the Navier solution is considered for the displacement components and rotation using the time harmonic function and harmonic solution along the plate length.

In summary, the results demonstrate that the structural stability of FGM sandwich nanoplates is highly sensitive to material gradation, geometric parameters, and nonlocal effects. The ceramic-rich composition (lower p values) enhances buckling resistance, while variations in thickness ratio (ζ_3) and incline angle (θ) exhibit nonlinear trends, with critical intersection points dictating their influence on structural performance. Additionally, the softening effect associated with the nonlocal parameter (e_0a) reduces buckling strength, whereas the hardening effect linked to the size parameter (l_m) improves it. These findings contribute to the optimization and design of advanced nanostructures for applications requiring superior thermal and mechanical performance in fields such as nanosensors, aerospace technology, and dental applications.

5. ACKNOWLEDGEMENTS

This study did not receive funding support from any institution or organization.

6. CONFLICT OF INTEREST

Author approves that to the best of their knowledge, there is not any conflict of interest or common interest with an institution/organization or a person that may affect the review process of the paper.

7. AUTHOR CONTRIBUTION

Adem Fatih OZALP has the full responsibility of the paper about determining the concept of the research, data collection, data analysis and interpretation of the results, preparation of the manuscript and critical analysis of the intellectual content with the final approval.

8. REFERENCES

Abuteir B. W., Boutagouga D., Free-vibration response of functionally graded porous shell structures in thermal environments with temperature-dependent material properties. Acta Mechanica 233(11), 4877-4901, 2022.

Akgöz B., Civalek Ö., Shear deformation beam models for functionally graded microbeams with new shear correction factors. Composite Structures 112, 214-225, 2014.

Al-Waily M., Raad H., Njim E. K., Free Vibration Analysis of Sandwich Plate-Reinforced Foam Core Adopting Micro Aluminum Powder. Physics and Chemistry of Solid State 23(4), 659-668, 2022.

Arani A. G., Jalaei M. H., Investigation of the longitudinal magnetic field effect on dynamic response of viscoelastic graphene sheet based on sinusoidal shear deformation theory. Physica B: Condensed Matter 506, 94-104, 2017.

Arslan K., Gunes R., Experimental Damage Evaluation of Honeycomb Sandwich Structures With Al/B4c FGM Face Plates Under High Velocity Impact Loads. Composite Structures 202, 304-312, 2018.

Boudjemai A., Bouanane M. H., Mankour A., Salem H., Hocine R., Amri R., Thermo-mechanical design of honeycomb panel with fully-potted inserts used for spacecraft design. 2013 6th International Conference on Recent Advances in Space Technologies (RAST), 39–46, Istanbul, Turkey: IEEE, 2013.

Chen X., Zhao J. L., She G. L., Jing Y., Luo J., Pu H. Y., On wave propagation of functionally graded CNT strengthened fluid-conveying pipe in thermal environment. European Physical Journal Plus 137(10), 2022.

Dang X. H., Nguyen V. L., Tran M. T., Tran B. D., Nguyen V. L., Nonlinear Dynamic Analysis of Auxetic-FGM Sandwich Plates Resting on a Kerr Elastic Substrate Under Blast Loading. Proceedings of the Institution of Mechanical Engineers Part C Journal of Mechanical Engineering Science 238(14), 6831-6846, 2024.

Gibson L. J., Cellular Solids. MRS Bulletin 28(4), 270-274, 2003.

Kiani Y., Eslami M. R., An exact solution for thermal buckling of annular FGM plates on an elastic medium. Composites Part B: Engineering 45(1), 101-110, 2013.

Kitipornchai S., Yang J., Liew K. M., Random vibration of the functionally graded laminates in thermal environments. Computer Methods in Applied Mechanics and Engineering 195(9-12), 1075-1095, 2006.

Lim C. W., Zhang G., Reddy J. N., A higher-order nonlocal elasticity and strain gradient theory and its applications in wave propagation. Journal of the Mechanics and Physics of Solids 78, 298-313, 2015.

Lin C., Nicaise S. M., Lilley D. E., Cortes J., Jiao P., Singh J., Bargatin I., Nanocardboard as a nanoscale analog of hollow sandwich plates. Nature Communications 9(1), 4442, 2018.

Markworth A. J., Ramesh K. S., Parks W. P., Modelling studies applied to functionally graded materials. Journal of Materials Science 30(9), 2183-2193, 1995.

Ozalp A. F., Esen I., Magnetic field effects on the thermomechanical vibration behavior of functionally graded biocompatible material sandwich nanobeams. Mechanics of Advanced Materials and Structures 32(3), 459-477, 2024.

Ozalp A. F., Esen I., Thermal buckling response of foam core smart sandwich nanoplates with electro-elastic and magneto-strictive layers. Acta Mechanica 236, 469-497, 2025.

Qi C., Jiang F., Yang S., Remennikov A., Chen S., Ding C., Dynamic Crushing Response of Novel Re-Entrant Circular Auxetic Honeycombs: Numerical Simulation and Theoretical Analysis. Aerospace Science and Technology 124, 107548, 2022.

Reddy J. N., A Simple Higher-Order Theory for Laminated Composite Plates. Journal of Applied Mechanics 51(4), 745-752, 1984.

Reddy J. N., Chin C. D., THERMOMECHANICAL ANALYSIS OF FUNCTIONALLY GRADED CYLINDERS AND PLATES. Journal of Thermal Stresses 21(6), 593-626, 1998.

Shimpi R. P., Refined Plate Theory and Its Variants. AIAA Journal 40(1), 137-146, 2002.

Thai H. T., Choi D. H., A refined plate theory for functionally graded plates resting on elastic foundation. Composites Science and Technology 71(16), 1850-1858, 2011.

Thai H. T., Choi D. H., A refined shear deformation theory for free vibration of functionally graded plates on elastic foundation. Composites Part B: Engineering 43(5), 2335-2347, 2012.

Thai H. T., Park T., Choi D. H., An efficient shear deformation theory for vibration of functionally graded plates. Archive of Applied Mechanics 83(1), 137-149, 2012.

Touloukian Y., Thermophysical properties of high temperature solid materials, Volume 3: Ferrous alloys. Macmillan: New York, 1967.

Van Lieu P., Zenkour A. M., Luu G. T., Static bending and buckling of FG sandwich nanobeams with auxetic honeycomb core. European Journal of Mechanics-A/Solids 103, 105181, 2024.

Wang Z. W., Zhang Q., Xia L. Z., Wu J. T., Liu P. Q., Thermomechanical Analysis of Pressure Vessels with Functionally Graded Material Coating. Journal of Pressure Vessel Technology 138(1), 011205, 2016.

Yang J., Liew K. M., Kitipornchai S., Stochastic analysis of compositionally graded plates with system randomness under static loading. International Journal of Mechanical Sciences 47(10), 1519-1541, 2005.

Yin H., Huang X., Scarpa F., Wen G., Chen Y., Zhang C., In-Plane Crashworthiness of Bio-Inspired Hierarchical Honeycombs. Composite Structures 192, 516-527, 2018.